Journal of Applied Polymer Science

Room temperature CO sensing by polyaniline/Co_3O_4 nanocomposite

T. Sen,[1] N. G. Shimpi,[2] S. Mishra[1]

[1]University Institute of Chemical Technology, North Maharashtra University, Jalgaon, Maharashtra, 425001, India

[2]Department of Chemistry, University of Mumbai, Kalina, Mumbai, Maharashtra 400098, India

Correspondence to: S. Mishra (E-mail: profsm@rediffmail.com)

ABSTRACT: Polyaniline/cobalt oxide (PANI/Co_3O_4) nanocomposites have been investigated for their sensitivity towards carbon monoxide (CO) gas at room temperature. The Co_3O_4 nanoparticles were prepared by ultrasound assisted coprecipitation method and then incorporated into the PANI matrix. Fourier transform infrared spectroscopy and ultraviolet–visible spectroscopy, powder X-ray diffraction, and field emission scanning electron microscopy have been used to characterize the nanomaterials. The PANI/Co_3O_4 nanocomposite sensors were found to be highly selective to CO gas at room temperature. A significantly high response of 0.81 has been obtained for 75 ppm CO concentration with a response time of 40 s. Based on the observations of the sensing study, a mechanism for CO sensing by the nanocomposite has been proposed. Influence of humidity on the sensor response towards CO has also been studied and the results presented. © 2016 Wiley Periodicals, Inc. J. Appl. Polym. Sci. **2016**, *133*, 44115.

KEYWORDS: conducting polymers; nanostructured polymers; sensors and actuators

Received 22 July 2015; accepted 22 June 2016

DOI: 10.1002/app.44115

INTRODUCTION

Over the years, nanomaterials have garnered the attention of the scientific community due to their exceptional properties and applicability in diverse fields.[1–6] In recent times, nanomaterials such as nanometals and nano-metal oxides have seen extensive usage as sensors in the field of electronics due to their excellent sensitivity as well as selectivity towards a range of analytes such as volatile organic compounds (VOCs),[7–9] toxic and inflammable gases,[9–13] and in quartz crystal microbalance sensors.[14] However, most of these nanometal and metal oxide-based sensors suffer from the disadvantage of having temperature-dependent sensitivity, i.e., they require high operating temperatures, which make them impracticable for use in ambient conditions. Hence, these nanomaterials need to be modified or combined with other materials to employ their excellent sensing ability for room temperature analyte detection. One of the ways of achieving this is through the use of intrinsically conducting polymers (ICPs) which are able to act as a matrix for such nanoparticles. Among the ICPs, polyaniline (PANI) has proved to be an excellent sensing element due to its modifiable electrical conductivity, good environmental stability, inexpensive monomer, and ease of synthesis.[15] PANI is a typical phenylene-based polymer having a chemically flexible —NH— group in the polymer chain flanked on either side by a phenylene ring.[16] Nanocomposites of PANI with nanometals[17–19] or nano-metal oxides[20–22] have shown good sensitivity towards a variety of VOCs and gases in ambient conditions. Also nano-dispersions of PANI are inkjet-printable directly on the substrate.[23] Amongst the various metal oxides incorporated in PANI for application as gas sensors, cobalt oxide (Co_3O_4) is a *p* type of semiconductor and is very attractive for applications involving oxidation reactions because of presence of mobile oxygen.[24] Co_3O_4 nanoparticles find applications in various fields like fuel cell,[25] high performance supercapacitor,[26] electrochemical cells,[27] batteries and gas sensors.[28] Despite such extensive studies, only a small body of work exits regarding room temperature detection of the highly toxic carbon monoxide (CO) gas[29–32] due to redox inactivity of CO at room temperature.

In our work, we investigate the viability of PANI/Co_3O_4 nanocomposite as a sensor for CO at room temperature. A binary dopant was used to increase the shelf life of the nanocomposite in its electrically conducting form. The Co_3O_4 nanoparticles were prepared via ultrasound assisted coprecipitation method and then incorporated into the PANI matrix. The nanocomposite was characterized using Fourier transform infrared spectroscopy (FTIR), UV–visible spectroscopy (UV–vis), X-ray diffraction (XRD), and field emission scanning electron microscopy (FESEM). The gas sensing measurements were made for different concentrations of CO in a "static" gas sensing setup. Humidity dependence of the nanocomposite sensor was also studied and the results are discussed.

EXPERIMENTAL

Materials

All the chemicals were of analytical grade and used as received. Aniline and ammonium persulphate (APS) were procured from

Thermo Fisher Scientific, Mumbai, India . Cobalt (II) chloride ($CoCl_2$), hydrochloric acid (HCl), and β-cyclodextrin (β-CD) were obtained from HiMedia Laboratories Pvt. Ltd., Mumbai, India. Sodium hydroxide (NaOH) was purchased from RFCL Ltd., Mumbai, India. Conducting silver paste was purchased from Sigma Aldrich, USA. 18 MΩ ultrapure water from Smart2-Pure system (Thermo Electron LED GmbH, Germany) was used for preparing solutions and for washing purposes.

Pretreatment of Glass Slides

Before film deposition the microscope glass slides (Polar India Corporation, Mumbai) were cleaned by immersing them in 0.1 *M* aqueous HCl solution for an hour. The slides were then successively sonicated in water and methanol using an ultrasonic probe (BO3 Ultrasonic Processor UP 1200, Cromtech, India) for 15 min each and finally vacuum dried.

Synthesis of Co_3O_4 Nanoparticles

Co_3O_4 nanoparticles were synthesized by drop-wise addition of an excess of aqueous NaOH solution to an aqueous solution of 0.08 *M* cobaltous chloride ($CoCl_2$) under ultrasound. The coprecipitation reaction was carried out in an ice bath. The appearance of rose–red colored precipitate indicated formation of cobalt (II) hydroxide ($Co(OH)_2$). After complete addition of NaOH, the reaction mixture was sonicated for an additional half an hour. Thereafter, the precipitate was centrifuged at 8000 rpm for 10 min and washed several times with water followed by a final rinsing in acetone. The nanoparticles were then dried at 80 °C and finally annealed at 400 °C for 1 h to obtain black colored Co_3O_4 nanoparticles.

Synthesis of PANI/HC/Co_3O_4 Nanocomposites

Since conventional protonic acid dopant-like HCl tends to escape from PANI with time resulting in a short shelf life of the conducting form of the polymer, therefore a binary dopant was employed in the synthesis of PANI and its nanocomposite. The binary dopant used was a solution of β-CD in 1 *M* aqueous HCl solution. Aniline was dissolved in this HCl/β-CD (HC) binary dopant solution with vigorous stirring. A predetermined amount of Co_3O_4 nanoparticles were then dispersed in the aniline/binary dopant aqueous solution by sonication. Pretreated glass slides were placed in the beaker containing the Co_3O_4/aniline/binary dopant solution for in situ deposition of nanocomposite films. An aqueous solution of APS (initiator) in 1 *M* HCl was then added drop-wise to the monomer solution under continuous stirring at room temperature (30 ± 2 °C). After complete addition of APS, the polymerization mixture was stirred for an additional hour and then left to stand overnight at room temperature. Thereafter, the glass slides were retrieved at a speed of 0.1 mm/min (the slow rate of retrieval being necessary to prevent striation on the film surface), washed with water and methanol, and vacuum dried for 30 min. The dark green precipitate of the nanocomposite was filtered, repeatedly washed with water, air-dried and finally vacuum dried at 60 °C for 6 h.

Three separate batches of PANI nanocomposites doped with HCl/β-CD binary dopant were prepared with varying Co_3O_4 nanoparticle content of 1, 2, and 3 wt %, which are henceforth referred as PANI/HC/C1, PANI/HC/C2, and PANI/HC/C3, respectively. PANI doped with binary dopant was also prepared and referred as PANI/HC throughout the text.

Characterization

Fourier Transform Infrared Spectroscopy. FTIR spectra of PANI/HC/Co_3O_4 nanocomposites were recorded on Shimadzu FTIR-8400 spectrophotometer (Tokyo, Japan) within the wavenumber range of 400–4000 cm^{-1}. The powdered samples (precipitate) were prepared in the pellet form by mixing with potassium bromide (KBr).

UV–Visible Spectroscopy. UV–vis absorption spectra of PANI/HC/Co_3O_4 nanocomposite films deposited on glass substrate were recorded on a Hitachi U-2900 spectrophotometer (Tokyo, Japan) in the range of 300–850 nm.

Field Emission Scanning Electron Microscopy. A Hitachi S-4800 field emission scanning electron microscope (Tokyo, Japan) was used to assess the morphology of Co_3O_4 nanoparticles and films of PANI/HC/Co_3O_4 nanocomposites. The samples were given a gold coating and mounted on a specimen stub before viewing under the microscope. Elemental analysis of the nanocomposite was performed using energy dispersive X-ray (EDX).

X-ray Diffraction. XRD analyses of Co_3O_4 nanoparticles and PANI/HC/Co_3O_4 nanocomposites powder were conducted on Brukers D8 Advance X-ray diffractometer (Brukers, Germany) with CuKα_1 radiation ($\lambda = 1.5404$ Å) within the 2θ range of 20–80°.

Gas Sensing Measurements. For the gas sensing studies, PANI/HC/Co_3O_4 nanocomposite films were loaded in a sensing chamber with two conducting probes placed in contact with the sensor surface through conducting silver paste. The other ends of the probes were connected to a DC power supply and a digital multimeter (Model SM5015, Scientific, Pune, India) through which the current flow within the sensors were recorded in the forward bias mode at a constant voltage. Predetermined amount of gas was introduced into the sensing chamber using a syringe and the sensor response and recovery were measured in air. The sensor response to CO was deduced from eq. (1)

$$R = \frac{(I_g - I_a)}{I_a} \quad (1)$$

where, R is response, I_a is current of sample in air, and I_g is current of sample in gas. All the electrical measurements were taken at ambient condition (room temperature 30 ± 2 °C and relative humidity (RH) of ∼20%). A pictorial representation of two-probe gas sensing setup is presented in Figure 1.

RESULTS AND DISCUSSION

Functional Group Identification by FTIR

Figure 2 shows the FTIR spectra of PANI/HC/Co_3O_4 nanocomposites. The main peaks observed in PANI/HC/C1 nanocomposite are 1514 and 1481 cm^{-1} corresponding to the quinoid and benzenoid ring stretching, which show the aromatic structure of PANI. The peaks at 3736 and 2978 cm^{-1} are associated with —N—H and —C—H stretching vibrations, respectively. The band at 1240 cm^{-1} can be assigned to bipolaron structure related to C—N bond stretching of secondary aromatic amine, while the band at 829 cm^{-1} corresponds to the aromatic out-of-plane C—H bending. Absorption bands corresponding to the stretching vibrations

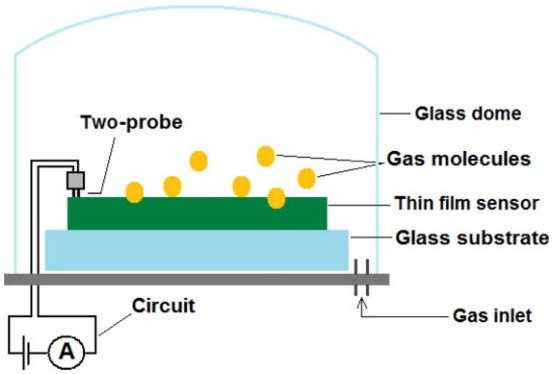

Figure 1. Pictorial representation of a two-probe gas sensing setup. [Color figure can be viewed in the online issue, which is available at wileyonlinelibrary.com.]

of C—H and C—O bonds in β-CD are observed at 2866 and 1132 cm^{-1}, respectively. The absorption bands appearing below 1000 cm^{-1} belonged to the metal–oxygen stretching vibrations. The broad bands at 657 and 596 cm^{-1} could be attributed to the Co—O bond stretching where Co^{3+} ion occupied the octahedral and tetrahedral positions, respectively.[33] A shift in absorption bands were observed at higher Co_3O_4 nanoparticle content, for example, the absorption bands for quinoid and benzenoid structures shifted to 1510 and 1427 cm^{-1} in PANI/HC/C3 while that of bipolaron structure related to C—N bond stretching of secondary aromatic amine shifted to 1288 cm^{-1}. Such a shift in the position of these bands appears to arise from the finite size effects of the Co_3O_4 nanoparticles wherein they interact with the neighboring PANI chains due to the presence of dangling bonds on the surface of the Co_3O_4 nanoparticles. The absorption near 2400 cm^{-1} corresponds to the CO_2 which appears due to the instrument's detection conditions.[34,35]

UV–Visible Spectroscopic Studies

The UV–visible spectra of the nanocomposite films are shown in Figure 3. The signature transition in PANI arising out of π–π* interaction was observed around 320–340 nm; in PANI/HC/C1 π–π* transition was observed at ~320 nm while in PANI/HC/C2 and PANI/HC/C3 it was found to be red-shifted

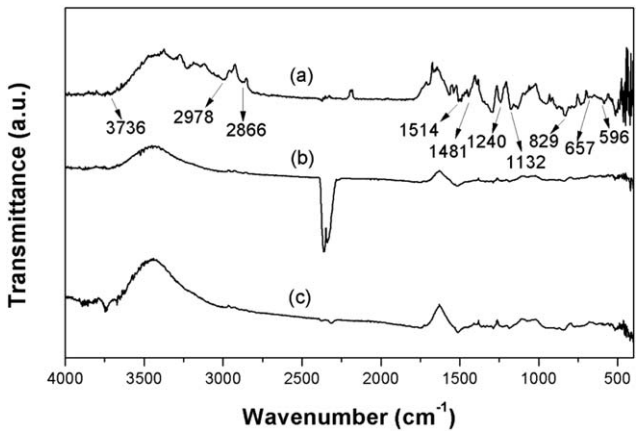

Figure 2. FTIR spectra of (a) PANI/HC/C1, (b) PANI/HC/C2, and (c) PANI/HC/C3 nanocomposites.

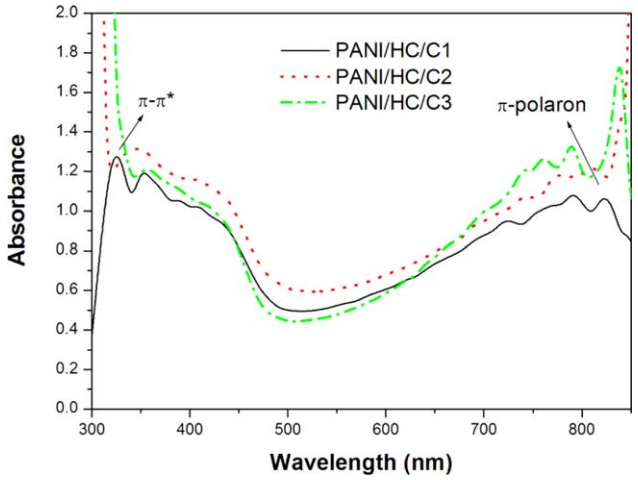

Figure 3. UV–visible spectra of PANI/HC/Co_3O_4 nanocomposites films. [Color figure can be viewed in the online issue, which is available at wileyonlinelibrary.com.]

to 334 and 340 nm. The π–polaron transitions in PANI are indicative of a strong interaction between the adjacent polarons leading to the polaron band becoming more delocalized and appearing at a longer wavelength. The π–polaron transitions in PANI/HC/C1, PANI/HC/C2, and PANI/HC/C3 were observed at 820, 810, and 790 nm, respectively. In its emeraldine base form (nonconducting) the π–polaron transition in PANI appears around 600 nm. The emeraldine salt results in a bathochromic shift in π–polaron transition which is characteristic of doped PANI. The observations from the UV–vis not only indicates an electrically conducting state of the PANI/HC/Co_3O_4 nanocomposite films but also signifies a lowering in π–polaron interaction possibly owing to an increased Co_3O_4 nanoparticle content. The change in peak positions for the π–polaron transitions in the nanocomposites towards a possible interaction between the Co_3O_4 nanoparticles and the quinoid groups of the polymer. With decrease in the concentration of Co_3O_4 nanoparticles in the PANI matrix, the absorbance peaks shift towards lower wavelength and the absorbance corresponding to the π–polaron transitions also decreases. This indicates an increase in the band gap of the nanocomposite which may be due to the introduction of an energy level corresponding to the Co_3O_4 nanoparticles in the band gap of PANI. It enables the electron charge transfer between the conduction band of Co_3O_4 and quinoid group of PANI easily. Thus, the charge transfer in PANI/HC/C1 is more encouraging than in PANI/HC/C2 and PANI/HC/C3.

Determination of Size and Morphology

Figure 4(a–d) presents the FESEM micrographs of Co_3O_4 nanoparticles and PANI/HC/Co_3O_4 nanocomposites films. Nanospheres of Co_3O_4 with a uniform average diameter of 23.4 nm were observed, which shows the effectiveness of ultrasound in producing nonaggregated nanoparticles even in the absence of an encapsulating agent. Nanofibrillar morphology was exhibited by PANI/HC/Co_3O_4 nanocomposites. At 1 wt % Co_3O_4 nanoparticle content the average diameter of the nanofibers were found to be ~80.6 nm. With increasing Co_3O_4 nanoparticle

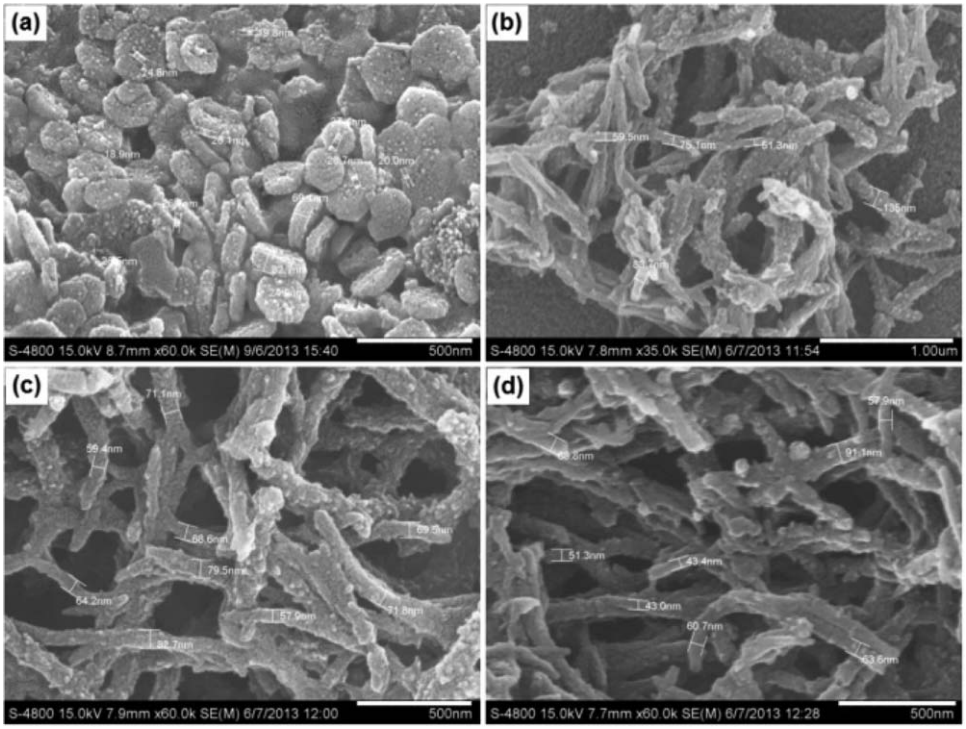

Figure 4. FESEM micrograph of (a) Co_3O_4 nanoparticles and PANI/HC/Co_3O_4 nanocomposites with Co_3O_4 nanoparticle content of (b) 1 wt %, (c) 2 wt %, and (d) 3 wt %.

content the average diameter size of the nanofibers decreased with PANI/HC/C2 and PANI/HC/C3 showing smaller diameters at ~68.8 and 59.5 nm, respectively. It thus appears that the Co_3O_4 nanoparticles play a significant role in guiding the formation of PANI nanofibers. Moreover, the surface of the PANI/HC/Co_3O_4 nanocomposites was observed to be rough

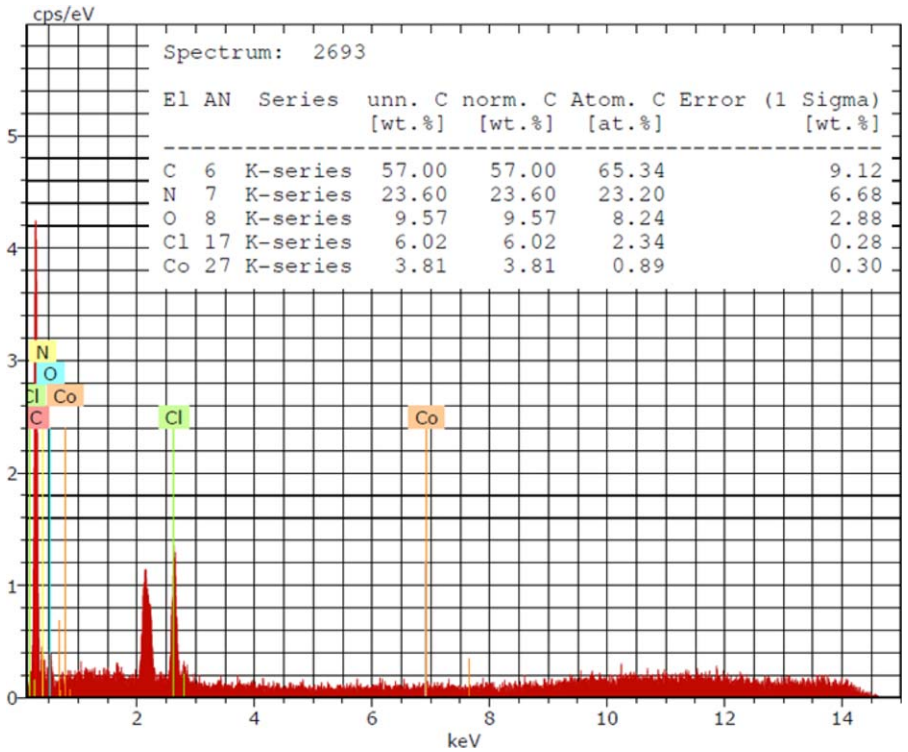

Figure 5. EDX spectra of PANI/HC/Co_3O_4 nanocomposite with 3 wt % Co_3O_4 nanoparticle content. [Color figure can be viewed in the online issue, which is available at wileyonlinelibrary.com.]

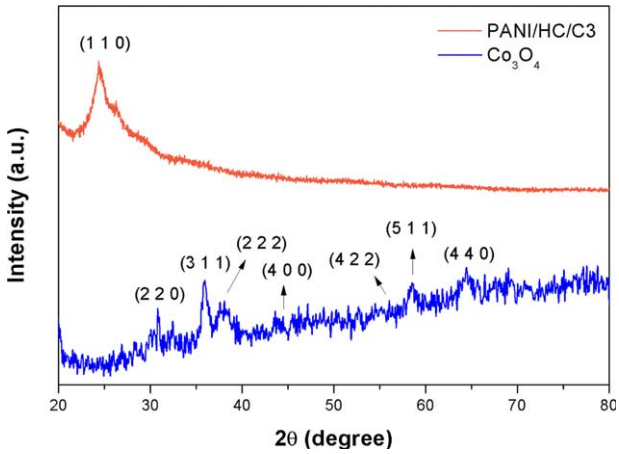

Figure 6. X-ray diffractogram of Co_3O_4 nanoparticles and PANI/HC/Co_3O_4 nanocomposites. [Color figure can be viewed in the online issue, which is available at wileyonlinelibrary.com.]

with polymer growth indicating towards the possibility of secondary growth of polymer on the surface of the already formed nanofibers induced by the presence of Co_3O_4 nanoparticles. The presence of Co_3O_4 nanoparticles in the PANI matrix is evident from the EDX spectra of PANI/HC/C3 nanocomposite (Figure 5).

Phase Identification by XRD

X-ray diffractogram of Co_3O_4 nanoparticles and PANI/HC/C3 nanocomposite are shown in Figure 6. The observed peaks in Co_3O_4 nanoparticles can be indexed to that of face-centered cubic phase of Co_3O_4.[36] The lattice constant for the Co_3O_4 nanoparticles was recorded as 0.8065 nm. The crystallite size of these nanoparticles, as calculated using Scherrer's equation, was found to be 23.29 nm, which is in excellent agreement with the FESEM data. The PANI/HC/C3 nanocomposites showed a sharp diffraction peak at ~24.5°, which is associated with (1 1 0) plane of PANI. The absence of Co_3O_4 nanoparticle diffraction peak suggests that the nanoparticles are embedded within the polymer matrix and are not present on the polymer surface.

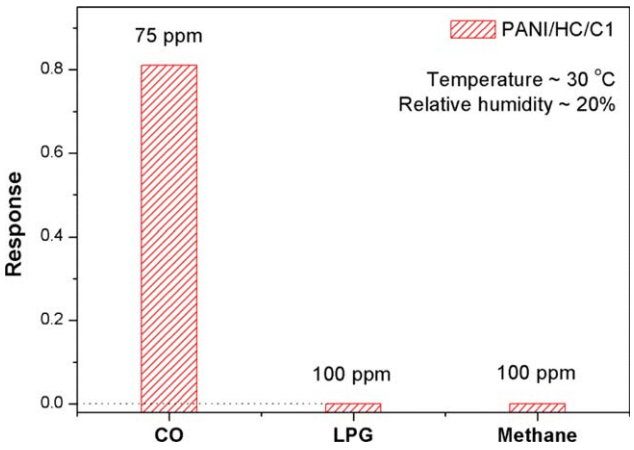

Figure 7. Selectivity bar graph of PANI/HC/Co_3O_4 nanocomposites for different gases. [Color figure can be viewed in the online issue, which is available at wileyonlinelibrary.com.]

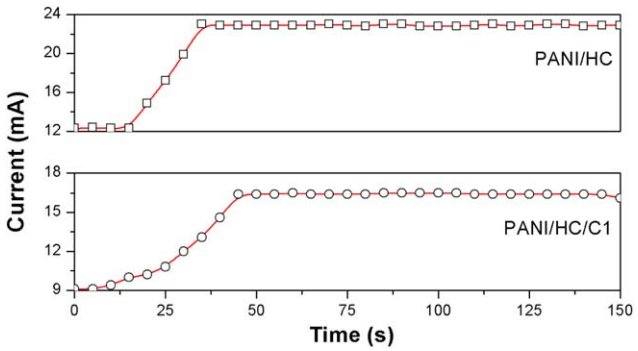

Figure 8. Current versus time graph of PANI/HC and PANI/HC/C1 for 75 ppm of CO. [Color figure can be viewed in the online issue, which is available at wileyonlinelibrary.com.]

CO Sensing Studies of PANI/HC/Co_3O_4 Nanocomposites

Sensing of CO at room temperature is a practical approach in assessment of sensor response in presence of atmospheric gases. The selectivity of the PANI/HC/Co_3O_4 nanocomposite sensor towards CO was assessed by comparing its response to methane and liquefied petroleum gas (LPG) at room temperature (Figure 7). No gas response was obtained in case of LPG and methane (both at 100 ppm concentration) by PANI/HC/C1 in ambient condition. However, a high gas response of ~0.8 was recorded for CO gas. This data signifies the high selectivity of PANI/HC/Co_3O_4 nanocomposites towards CO amongst the test gases. On this basis further investigations were carried out on the sensor response and recovery towards different CO concentrations.

The sensing ability of PANI-based nanocomposite sensor manifests as a change in its current, and consequently, in its resistance. Depending on the nature of analyte, the resistance of PANI either increases or decreases. The character of PANI/HC/Co_3O_4 nanocomposite sensor was determined by recording the current versus time graph of PANI/HC and PANI/HC/C1 for different concentrations of CO (Figure 8). A sharp increase in current was registered when the sensor was exposed to CO gas resulting in an increase in conductivity of the sensor, which indicates an increase in charge carriers in PANI. On the basis of this observation, the sensing mechanism is proposed to be a partial electron transfer between the CO gas and the polymer.[30] The stable resonance structure of $^{+}C{\equiv}O^{-}$ withdraws the lone pair of electron from the amine nitrogen (—NH—) in PANI, thus transferring the positive charge from the carbon of CO to the amine nitrogen of PANI. This results in an increase in hole concentration in the polymer (charge carriers in PANI) which consequently increases its conductivity.

Figures 9 and 10 shows the response versus time curve of PANI/HC/Co_3O_4 nanocomposites for 50 and 75 ppm CO concentrations, respectively. The gas response was recorded by introducing CO into the sensing chamber shown as "gas in" in Figures 9 and 10. The interaction between the sensor and the gas brings about a change in the sensor's conductivity. When no further change is observed in the sensor's response the gas was expunged from the chamber (shown as "gas out" in Figures 9 and 10) following which the sensor starts to recover its initial conductivity. In terms of sensor response towards CO, PANI/HC shows a slightly higher

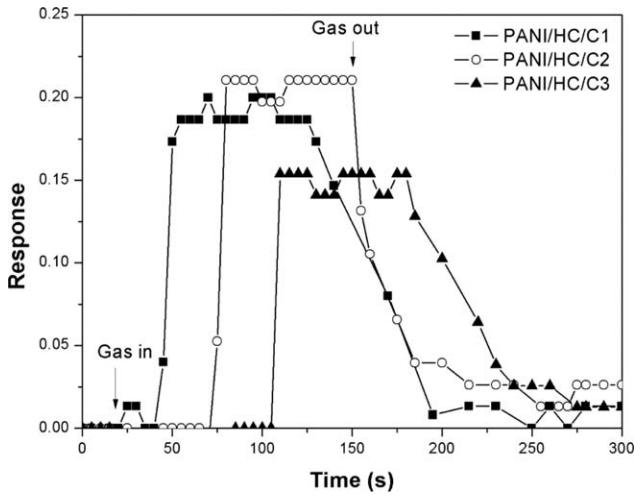

Figure 9. Response versus time graph of PANI/HC/Co_3O_4 nanocomposites at 50 ppm CO concentration.

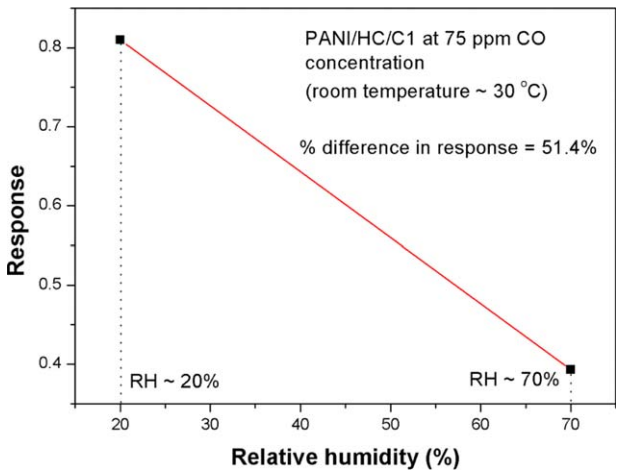

Figure 11. Humidity dependence of PANI/HC/C1 nanocomposite for 75 ppm CO concentration. [Color figure can be viewed in the online issue, which is available at wileyonlinelibrary.com.]

response factor (0.86) than PANI/HC/C1 (0.81) for 75 ppm CO. At 50 ppm CO concentration, PANI/HC does not show any response while for PANI/HC/C1 nanocomposite a response factor of 0.2 was recorded. PANI/HC/C2 and PANI/HC/C3 records a further drop in response at 0.75 and 0.34, respectively, towards 75 ppm CO concentration. The drop in sensor response as observed with increasing content of Co_3O_4 nanoparticles can be accounted by the increasing interaction between the Co_3O_4 nanoparticles and the PANI matrix, as distinctly indicated from the UV–visible spectra of the nanocomposite films. Such an interaction can possibly hinder the partial electron transfer process taking place between the analyte and the sensor, which ultimately leads to lowering of the sensor response. PANI/HC/Co_3O_4 nanocomposite at 1 wt % Co_3O_4 nanoparticle content thus shows a higher response than the 2 and 3 wt % nanocomposites.

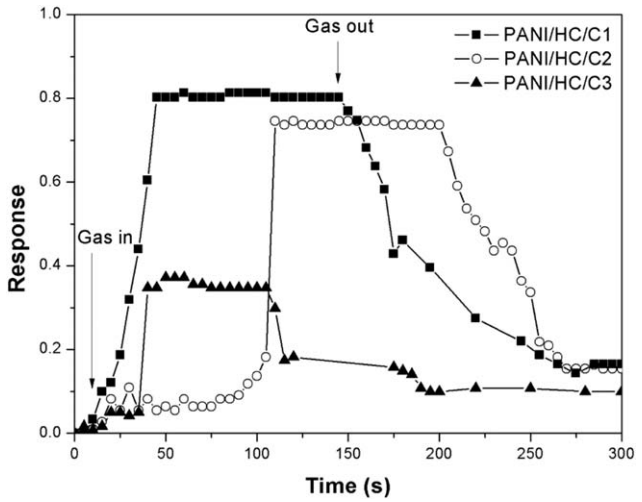

Figure 10. Response versus time graph of PANI/HC/Co_3O_4 nanocomposites at 75 ppm CO concentration.

Besides the sensor's response towards the analyte, the response and recovery times of the sensor were also recorded. The response time of the PANI/HC/C1 nanocomposite was found to be 40 s for 75 ppm CO concentration and 45 s for 50 ppm CO concentration. The recovery time for PANI/HC/C1 nanocomposite sensor was higher at 140 and 90 s for 75 and 50 ppm CO concentrations, respectively. The longer recovery time for the nanocomposites can be explained as a result of faster desorption of gas molecules at the sensor surface owing to the hindrance in the electron transfer process between the gas and the nanocomposite due to higher Co_3O_4 nanoparticle content, which is in agreement with the results obtained from UV–vis. The electron transfer in PANI/HC/C1 is easier than that it PANI/HC/C2 and PANI/HC/C3.

Several CO sensors have been reported in the literature with different testing conditions eliciting different responses. Tripathy and Hota[37] reported a tin oxide (SnO_2) sensor with a high response factor of ~60 that was obtained at a temperature of 200 °C. However, high temperature sensing is neither a safe nor a practical approach in all cases and has therefore generated interest in the area of room temperature sensing of gases. Amongst these, there has been a report of SnO_2 nanoparticle decorated single-walled carbon nanotubes (SWCNTs) for room temperature CO detection[38] in which the authors reported the highest response to be 0.27 for 100 ppm CO concentration. Another SWCNT-based sensor reported a response factor <0.014 for 50 ppm CO concentration at room temperature.[39] It should be noted that in these cases the sensor response is much lower than that reported by us.

The effect of humidity on the sensor response was also determined by taking the current measurements at different RH levels of ~20 and 70% for 75 ppm CO (Figure 11). A drastic drop in sensor response was observed for increased humidity level. This could be owing to the polarization of water molecules near the PANI surface at high humidity levels, which leads to formation of attractive forces between water molecules and the

polymer. The subsequent thin layer of water that forms on the PANI surface acts as a barrier against CO adsorption resulting in lowering of sensor response.[40] The percentage difference in sensor response at the two humidity levels for PANI/HC/C1 was observed to be ~51.4%. The result thus shows a significant humidity dependence of PANI/HC/Co_3O_4 nanocomposite sensor towards CO.

CONCLUSIONS

PANI/HC/Co_3O_4 nanocomposites were prepared by chemical polymerization of aniline in presence of Co_3O_4 nanoparticles. The nanocomposites were doped with HCl/β-CD binary dopant to increase the life of the nanocomposites in doped form. FESEM micrographs revealed successful formation of size-controlled Co_3O_4 nanoparticles (~23 nm in size) by the ultrasound assisted synthesis method; PANI was observed to have nanofibrillar morphology. The gas sensing studies suggest a partial electron transfer mechanism between the CO molecules and PANI moieties. PANI/HC/C1 exhibited a significantly high response to CO at a concentration as low as 75 ppm with a short response time. Unlike pristine PANI (PANI/HC), the nanocomposites were found to be sensitive to 50 ppm CO as well. The nanocomposite sensor exhibited excellent selectivity towards CO. However, the sensor also suffer from certain limitations such as a drop in sensor response with increasing Co_3O_4 nanoparticle content that has been attributed to a hindrance in the partial electron transfer process due to the presence of Co_3O_4 nanoparticles. In addition, the sensor also displayed high humidity dependence which further impedes its performance. Therefore, further modifications in the composition of the nanocomposite sensor are necessary to counter its limitations in its present form. Nevertheless, the sensor fabrication as reported in this work is one that is both facile and economical which, coupled with significant performance has much potential in the field of gas sensors.

ACKNOWLEDGMENTS

One of the authors (T. Sen) is thankful to the University Grants Commission, New Delhi, India for providing financial support under the RFSMS scheme.

REFERENCES

1. Mishra, S.; Shimpi, N. G.; Mali, A. D. *Polym. Adv. Technol.* **2011**, *23*, 236.
2. Mishra, S.; Shimpi, N. G.; Mali, A. D. *Polym. Plast. Technol. Eng.* **2011**, *50*, 758.
3. Agrawal, S.; Parveen, A.; Azam, A. *Mater. Lett.* **2016**, *168*, 125.
4. Mishra, S.; Sonawane, S.; Mukherji, A.; Mruthyunjaya, H. C. *J. Appl. Polym. Sci.* **2006**, *100*, 4190.
5. Sung, S.; Kim, D. S. *J. Appl. Polym. Sci.* **2013**, *129*, 1340.
6. Chaudhari, P.; Chaudhari, V.; Mishra, S. *Mater. Res.* **2016**, *19*, 446.
7. Parmar, M.; Rajanna, K. *Int. J. Smart Sens. Intell. Syst.* **2011**, *4*, 710.
8. Chen, Y. J.; Xue, X. Y.; Wang, Y. G.; Wang, T. H. *Appl. Phys. Lett.* **2005**, *87*, 233503.
9. Dhayal Raj, A.; Pazhanivel, T.; Suresh Kumar, P.; Mangalaraj, D.; Nataraj, D.; Ponpandian, N. *Curr. Appl. Phys.* **2010**, *10*, 531.
10. Chang, S. J.; Weng, W. Y.; Hsu, C. L.; Hsueh, T. *J. Nano Commun. Networks* **2010**, *1*, 283.
11. Chaudhari, P.; Mishra, S. *Measurement* **2016**, *90*, 468.
12. Patil, D. R.; Patil, L. A.; Patil, P. P. *Sens. Actuators B* **2007**, *126*, 368.
13. Dhingra, M.; Singh, N. K.; Shrivastava, S.; Senthil Kumar, P.; Annapoorni, S. *Sens. Actuators A* **2013**, *190*, 168.
14. Yang, M.; He, J.; Hu, X.; Yan, C.; Cheng, Z. *Environ. Sci. Technol.* **2011**, *45*, 6088.
15. Mishra, S.; Shimpi, N. G.; Sen, T. *J. Polym. Res.* **2013**, *20*, 49.
16. Shinde, S.; Kher, J. *Int. J. Innov. Res Sci. Eng. Technol.* **2014**, *3*, 16570.
17. Barkade, S. S.; Naik, J. B.; Sonawane, S. H. *Colloids Surf. A* **2011**, *378*, 94.
18. Sharma, S.; Nirkhe, C.; Pethkar, S.; Athawale, A. A. *Sens. Actuators B* **2002**, *85*, 131.
19. Athawale, A. A.; Bhagwat, S. V.; Katre, P. P. *Sens. Actuators B* **2006**, *114*, 263.
20. Huyen, D. N.; Tung, N. T.; Thien, N. D.; Thanh, L. H. *Sensors* **2011**, *11*, 1924.
21. Sen, T.; Shimpi, N. G.; Mishra, S.; Sharma, R. P. *Sens. Actuators B* **2014**, *190*, 120.
22. Lina, G. *Trans. Nonferrous Met. Soc. Chin.* **2009**, *19*, s678.
23. Crowley, K.; Smyth, M.; Killard, A.; Morrin, A. *Chem. Pap.* **2013**, *67*, 771.
24. Ozkaya, T.; Baykal, A.; Koseoglu, Y.; Kavas, H. *Cent. Eur. J. Chem.* **2009**, *3*, 410.
25. Irankhah, R.; Raissi, B.; Maghsoudipour, A. *Iranian J. Hydrogen Fuel Cell* **2014**, *2*, 121.
26. Liu, H.; Gou, X.; Wang, Y.; Du, X.; Quan, C.; Qi, T. *J. Nanomater.* **2015**, *2015*, 8744245.
27. Simon, P.; Gogotsi, Y. *Nat. Mater.* **2008**, *7*, 845.
28. Li, W.; Xu, L.; Chen, J. *Adv. Funct. Mater.* **2005**, *15*, 851.
29. Misra, S. C. K.; Mathur, P.; Srivastava, B. K. *Sens. Actuators A* **2004**, *114*, 30.
30. Choi, H. H.; Lee, J.; Dong, K. Y.; Ju, B. K.; Lee, W. *Macromol. Res.* **2012**, *20*, 143.
31. Ullah, H.; Anwar-ul-Haq, A. S.; Bilal, S.; Ayub, K. *J. Phys. Chem. C* **2013**, *117*, 23701.
32. Kim, D.; Pikhitsa, P. V.; Yang, H.; Choi, M. *Nanotechnology* **2011**, *22*, 485501.
33. Tang, C. W.; Wang, C. B.; Chien, S. H. *Thermochim. Acta* **2008**, *473*, 68.
34. http://web.mit.edu/5.32/www/Appendix_1_Qual_Instrumentation_03.pdf.

35. Rinsland, P.; Smith, M.; Russell, J.; Park, J.; Farmer, C. *Appl. Opt.* **1981**, *20*, 4167.
36. Dong, Y.; He, K.; Yin, L.; Zhang, A. *Nanotechnology* **2007**, *18*, 435602.
37. Tripathy, S. K.; Hota, B. P. *African Rev. Phys.* **2012**, *7*, 47.
38. Zhang, Y.; Cui, S.; Chang, J.; Ocola, L. E.; Chen, J. *Nanotechnology* **2013**, *24*, 025503.
39. Hannon, A.; Lu, Y.; Li, J.; Meyyappan, M. *J. Sens. Sens. Syst.* **2014**, *3*, 349.
40. Azim-Araghi, M. E.; Jafari, M. J. *Eur. Phys. J. Appl. Phys.* **2010**, *52*, 10402.